



# Machine learning-driven predictive modeling of temperature-dependent mechanical properties in austenitic stainless steels

Movaffaq Kateb<sup>a,\*</sup>, Sahar Safarian<sup>b</sup>

<sup>a</sup> Structural Chemistry Division, Department of Chemistry-Ångström Laboratory, Uppsala University, Lägerhyddsvägen 1, P.O. Box 538, 75121 Uppsala, Sweden

<sup>b</sup> IVL Swedish Environmental Research Institute, Aschebergsgatan 44, 41133 Gothenburg, Sweden

## ARTICLE INFO

### Keywords:

Austenitic stainless steel  
Machine learning  
Mechanical properties  
Nonlinear temperature-dependent  
Random forest  
SHAP

## ABSTRACT

This work demonstrates that modern tree-based models can effectively model complex, temperature-dependent mechanical responses, including highly nonlinear and even non-monotonic trends, in austenitic stainless steel and highlights limitations of composition-only empirical models. To ensure robust model evaluation, we employed multiple validation strategies including repeated random train and test partitions and leave-one-out cross-validation. While one might assume that steel grade is fully captured by its composition, local assessments within narrower compositional ranges reveal different feature importance rankings than those observed in the full dataset. Grade-specific (AISI 304, 316, 321 and 347) feature importance analysis offered deeper insights into local alloy behavior and demonstrated the advantage of disaggregated modeling in avoiding misleading conclusions. Clustering and SHAP analyses further revealed a temperature-sensitive role of nitrogen, which strengthens the alloy through interstitial and fine precipitate mechanisms at lower temperatures but loses effectiveness at elevated temperatures due to precipitate coarsening. This highlights how data-driven methods can uncover metallurgically consistent, temperature-dependent strengthening behaviors not captured by simpler models. Our results confirm that temperature governs the mechanical performance of austenitic stainless steels, with other features contributing marginally, particularly for UTS. Additionally, the model achieved a notably high score for elongation, highlighting the critical role of testing temperature in addressing the long-standing challenge of poor elongation predictions in composition-only or composition-processing models. This suggests that low accuracy in previous studies is more likely due to dataset limitations rather than shortcomings of tree-based models.

## 1. Introduction

Addressing climate change demands urgent transformation across heavy industries and steel production, stands at the center of this challenge. In Sweden, sustainability has long guided the steel industry, which has relied on recycled scrap for over 80 years and is now pioneering fossil-free steelmaking (Safarian, 2023). Yet, balancing environmental responsibility with the demand for high-performance steels presents increasing complexity, particularly as alloy systems and processing routes grow more sophisticated. While artificial intelligence (AI) has shown promise in accelerating materials discovery, their integration into steel development remains limited in scope and often lacks engineering interpretability (Kateb & Safarian, 2025). There is a growing need for AI frameworks that not only advance scientific understanding but also align with industrial and societal imperatives (Safarian et al.,

2020, 2021a, 2021b).

Within this broader effort, austenitic stainless steels emerge as a particularly important class due to their widespread industrial use and unique material characteristics. Their high Cr content enables self-passivation, giving rise to excellent corrosion resistance while balancing cost, strength and service life, making it ideal for applications in the home appliances, food and beverage, pharmaceutical and chemical industries. These alloys retain their face-centered cubic (FCC) *austenite* phase over a wide temperature range, making them especially valuable for high-temperature environments such as power generation and heat exchangers, furnaces, engine parts and exhaust, petrochemical and refinery equipment (Quaranta & Davies, 2022; Safarian, 2023). This is thanks to the presence of austenite-stabilizing elements such as Ni, Mn and N. Notably, nickel is the most effective stabilizer at ambient conditions; the Ni-Fe phase diagram reveals a dominant FCC structure even

\* Corresponding author.

E-mail addresses: [movaffaq.kateb@kemi.uu.se](mailto:movaffaq.kateb@kemi.uu.se) (M. Kateb), [Sahar.Safarianbana@ivl.se](mailto:Sahar.Safarianbana@ivl.se) (S. Safarian).

<https://doi.org/10.1016/j.mlwa.2025.100786>

Received 29 June 2025; Received in revised form 30 October 2025; Accepted 1 November 2025

Available online 6 November 2025

2666-8270/© 2025 The Author(s). Published by Elsevier Ltd. This is an open access article under the CC BY license (<http://creativecommons.org/licenses/by/4.0/>).

across intermetallic regimes (Kateb et al., 2019). The FCC crystal structure provides a high number of slip systems, which contributes to exceptional ductility and resistance to brittle fracture (Kateb et al., 2009; Kateb & Dehghani, 2012), an essential property for cryogenic applications. In addition, their excellent weldability and formability make them ideal for fabricating complex components like pipes, pressure vessels and structural assemblies.

Despite these advantages, optimizing austenitic stainless steels remains difficult due to the complex interplay of composition, microstructure and temperature. Austenitic grades exhibit significant work hardening and strain rate sensitivity, both strongly influenced by temperature (Norström, 1977). In presence of strain at elevated temperatures, the FCC structure may either transform into harder phases (Azadeh et al., 2019; Kateb et al., 2018; Kateb & Manolescu, 2023; Rahmati et al., 2014), or soften due to recovery and recrystallization (Colombier & Hochmann, 1967). While empirical models have primarily emphasized the role of composition (Balachandran et al., 2001; H. Nordberg, 1993; Irvine et al., 1969), the temperature-dependence of mechanical properties remains relatively underexplored (Norström, 1977). Therefore, investigating how key mechanical properties, such as yield strength (YS), ultimate tensile strength (UTS) and elongation (EI), evolve with temperature is not only scientifically relevant but also essential for the safe and optimized design of these steels.

To address this complexity, researchers have traditionally relied on linear regression models to characterize the strength of austenitic steels (Balachandran et al., 2001; H. Nordberg, 1993; Irvine et al., 1969; Norström, 1977). The interplay of composition, heat treatment and thermo-mechanical processing creates a vast parameter space with many hidden relationships, often imperceptible even to experts. Since the effects may not be strictly linear, extrapolation can be unreliable, a non-linear modeling approach is necessary to accurately capture the underlying relationships (Narayana et al., 2020; Shah, 2002).

Machine learning (ML) provides a promising alternative to uncover these hidden correlations, making it a powerful tool for optimization in high-dimensional design spaces. For instance, Xie et al. (2021) studied a large dataset (>11,000) of several steel grades using different models such as deep neural network (DNN), support vector machines (SVM), k-nearest neighbors (kNN) and random forest (RF). They pointed out SVM limitation for handling 27 variables. However, as Shen et al. (2019) reported, SVM performed well on a much smaller steel dataset but narrower parameter space. SVM is known to scale poorly with increasing dataset size, which has contributed to the growing popularity of RF (Shabani et al., 2025). Interestingly, RF has also become common practice for small datasets, a somewhat counterintuitive trend, since smaller datasets typically cannot accommodate many alloying or processing features without risking overfitting (Xiong et al., 2020). Nevertheless, researchers often opt to reduce the number of features while still relying on RF (Diao et al., 2022; C. C. Wang et al., 2020). This preference is largely due to RF's robustness against noise, a valuable trait when working with experimental data.

In various steels a strong correlation between composition and treatment has been observed upon ML analysis (S. Guo et al., 2019; Z. Guo & Sha, 2004). Thus, one can completely focus on the composition since many alloying elements take effect upon specific heat treatment followed by strict cooling protocols (Kateb & Safarian, 2025). The latter has been shown to deliver more meaningful results, rather skipping less important features that may cause poor generalization to new data and incorrect scientific or engineering conclusions. It is also possible to mix small datasets to remove bias to certain process parameter and prevent overfitting simultaneously (Kateb & Safarian, 2025; Xie et al., 2021; Xiong et al., 2020). These studies provide valuable insight into the composition–strength relationship under controlled conditions.

In parallel, temperature has emerged as another dominant factor influencing mechanical performance beyond composition-processing relationships. Its relevance extends beyond high-temperature safety to process design, including thermomechanical treatments, welding and

creep. Early studies revealed that temperature strongly influences strength, often more than composition. For example, Mandal et al. (2008) identified temperature and strain rate as the dominant factors of AISI 304 L. In a follow-up study, they reported a stronger correlation between composition and strength at constant temperature (Mandal et al., 2009), but also noted shifts in feature importance with temperature changes, again underscoring the dominant role of temperature. While earlier work focused on compressive behavior in a single grade, Narayana et al. (2020) extended the analysis to tensile data across several austenitic grades, confirming higher ML performance over empirical models when predicting strength at constant temperatures. Since then, the critical influence of temperature has been widely acknowledged (Liu et al., 2023; Wang et al., 2020b). More recently, Fajrul Falaakh et al. (2024) demonstrated that ML models, even without constant-temperature constraints, outperform empirical methods in predicting fatigue crack growth rates at high temperatures.

This study investigates the relationships between austenitic stainless-steel compositions, heat treatment and their resulting mechanical properties to uncover how individual feature influence performance. The dataset includes samples with identical compositions and heat treatments, measured at different temperatures, highlighting the temperature-dependence of mechanical properties, with a few critical aspects often overlooked in the existing literature. Unlike our previous study here we use a larger dataset that allows us to incorporate more features such as heat treatment. Earlier studies often relied on smaller subsets drawn from the same source data, limiting the generalizability of their findings. By exploring these interactions, the work aims to deepen understanding of the underlying mechanisms that govern material behavior and support the design of steels tailored for specific applications. We start with comparison of different models such as RF, SVM, extreme gradient boosting machines (XGB) (Chen & Guestrin, 2016) and artificial neural networks (ANN) (Safarian et al., 2020, 2021b, 2021a). Then we focus on the RF method and various cross validation method. Overall, this work contributes to the broader integration of ML in materials science and provides a practical framework for developing and optimizing high-performance steel alloys.

## 2. Methodology

### 2.1. Data description

Data on 2180 samples, AISI 304, AISI 316, AISI 321 and AISI 347 stainless steels was utilized for this study to develop the ML model. The dataset includes experimental uniaxial tension measurements of austenitic steels, originally compiled by Shah and Sourmail (2002) within the materials algorithm project (MAP) at the University of Cambridge. The dataset references indicate contributions from the British steelmakers creep committee and Japanese national research institute for metals, both known for generating high-quality, accurate and reliable data adhering to rigorous experimental and reporting standards. The MAP datasets are considered highly reliable, as they are curated by experts in materials modeling for the purpose of algorithm validation.

The dataset used in this study includes the actual weight percent of 16 key alloying elements found in steels, namely: aluminum, boron, carbon, chromium, cobalt, copper, manganese, molybdenum, nitrogen, nickel, niobium, phosphorus, silicon, sulfur, titanium and vanadium. Columns for lead, tantalum, tin, tungsten and zirconium were present but had zero values across all entries and were therefore excluded from analysis. Additional sample preparation information is included, such as the type of furnace used for melting, ingot size, product form and grain size. The data also includes solution treatment temperature (STT), solution treatment time (STt), post treatment quenching medium (QM) which was either air or water. Finally, the temperature at which uniaxial tension tests were conducted is provided, along with the resulting mechanical properties: 0.2 % proof stress (PS), ultimate tensile strength

(UTS), elongation (El) and area reduction (AR). In many materials, yielding occurs gradually, making the elastic limit difficult to define precisely. Thus, the PS, typically defined as the stress corresponding to a plastic strain of 0.002, is commonly used instead. The comment section in the dataset indicates for 199 samples, the reported Nb values represent the combined content of niobium and tantalum. Additionally, sulfur concentrations were missing in 155 samples and phosphorus in 171 samples. Due to the importance of these elements, default values of 0.021 wt % for sulfur and 0.013 wt % for phosphorus were assigned.

Grain size and ingot size were excluded from the analysis due to missing values in approximately 70 % of the samples. A similar level of missing values was observed for AR, but because it is strongly correlated with El, it was imputed with high accuracy. During data cleaning, two data points with unusually high elongation values (>400 %) were identified, likely due to typographical errors. These were removed following expert recommendations. The dataset's statistical summaries are presented in Tables 1–4. Table 1 shows the range, mean and standard deviation values for the 18 alloying elements included in the modeling. This reflects a much broader parameter space compared to similar studies, e.g. (Narayana et al., 2020). As previously mentioned, the study does not focus on a single steel grade, but rather includes a variety of austenitic stainless steel grades. Table 2 presents statistics of the uniaxial tension test results. The remaining sample conditions are categorized into numerical and categorical variables, summarized in Tables 3 and 4, respectively. Various imputation methods were evaluated, including RF, kNN and multiple imputation by chained equations (MICE). These did not yield meaningful differences in predictive performance. Given that several variables had a high proportion of missing values, up to 70 %, MICE was selected, as it converged more efficiently and provided stable imputations across iterations. One-hot encoding was used for all categorical variables.

## 2.2. Machine learning model development

To model and predict the mechanical properties of austenitic stainless steels, this study employed several well-established supervised ML algorithms, including RF, ANN, SVM and XGB. These models were selected for their proven capabilities in handling non-linear relationships and multivariate data typical of materials science problems. For each algorithm, a tailored hyperparameter optimization was carried out in two stages: an initial random search explored a broad space of hyperparameter combinations, followed by a refined grid search to fine-tune model settings based on the most promising regions identified. Model tuning was performed using 5-fold cross-validation applied to the training data to prevent overfitting and ensure generalizability. Search spaces and final parameters needed to reproduce our results can be found in Table 5 and 6. Among all models, RF exhibited strong baseline performance with minimal tuning, highlighting its robustness and efficiency, traits that made it a practical choice for further development.

To compare predictive performance of RF model, first the dataset was randomly partitioned into 80/20 train/test split (1-seed). Beyond single-split validation, a more extensive evaluation was performed

**Table 1**

Statistical values of alloying elements in austenitic stainless-steel samples. All values are in actual weight percent unit.

	Cr	Ni	Mo	Mn	Si	Nb	Ti	Cu
<b>Min</b>	15.9	8.4	0	0.61	0	0	0	0
<b>Max</b>	21.06	34.45	2.91	1.82	1.15	0.95	0.56	0.35
<b>Mean</b>	17.81	12.58	1.02	1.46	0.50	0.10	0.15	0.04
<b>Std Dev</b>	1.00	5.15	1.16	0.24	0.14	0.26	0.20	0.08
	N	C	B	P	S	Al	Co	V
<b>Min</b>	0	0.01	0	0	0	0	0	0
<b>Max</b>	0.08	0.12	0.02	0.04	0.05	0.52	0.54	0.06
<b>Mean</b>	0.01	0.06	0.0004	0.02	0.013	0.03	0.04	0.003
<b>Std Dev</b>	0.012	0.014	0.0010	0.008	0.007	0.10	0.10	0.01

**Table 2**

Statistical values of mechanical properties in austenitic stainless-steel samples as well as measurement temperature.

Property	PS/YS (MPa)	UTS (MPa)	El ( %)	RA ( %)	T (K)
<b>Min</b>	35	47	11	14	293
<b>Max</b>	341	714	505	97	1273
<b>Mean</b>	159	433	47	69	675
<b>Std Dev</b>	47	94	18	12	233
<b>NA</b>	0	0	95	1517	0

**Table 3**

Statistical values of heat treatment, microstructure and size in steel samples.

Property	STT (K)	STt (s)	Grain size (mm <sup>2</sup> )	Ingot size (unknown)
<b>Min</b>	1279	0	37	0.21
<b>Max</b>	1473	7200	1024	16
<b>Mean</b>	1361	1754	231	3.88
<b>Std Dev</b>	36	1904	229	3.52
<b>NA</b>	184	1097	1517	1517

**Table 4**

Categorical parameters mapping and their repetition.

Column	Value	Count
<b>QM</b>	Air quenched	1174
	Water quenched	742
	NA	264
<b>melt</b>	Basic electric arc furnace	1341
	High frequency induction furnace	445
	NA	217
	Electric furnace	177
<b>form</b>	Tube	1632
	Bar	259
	Plate	238
	Bloom	51

across 100 different random seeds (100-seeds) to ensure statistical robustness and the resulting prediction errors were summarized using mean and standard deviation metrics to capture variance introduced by data shuffling. In addition, leave-one-out cross-validation (LOOCV) was used to maximize the use of available data, training on all samples except one and testing on the excluded point in each iteration. This approach allowed for a thorough and unbiased assessment of model reliability. Since LOOCV requires a number of iterations equal to the number of data points, making it expensive for large dataset, we also evaluated RF performance using alternative validation strategies, including 5-fold, 20-fold and 100-fold cross-validations.

Feature importance was estimated using the mean decrease in impurity (MDI) from Random Forest regression models implemented in scikit-learn. This method measures the reduction in variance contributed by each feature when used in a tree split. To assess stability, the standard deviation of feature importance across all trees in the forest

**Table 5**

Hyperparameter tuning search spaces for each model, chosen based on preliminary experiments and literature.

Model	Parameters Tuned	Search Space
<b>ANN (MLPRegressor)</b>	Hidden layers	(50,), (100,), (100, 50)
	Activation	relu, tanh
	Solver	adam
	Regularization (alpha)	0.0001, 0.001, 0.01
	Max iterations	2000
<b>SVM (SVR)</b>	C (regularization)	0.01, 0.1, 1, 10, 100
	Epsilon	0.1, 0.2, 0.5
	Kernel	linear, rbf
<b>RF (RandomForestRegressor)</b>	-	defaults
<b>XGBoost (XGBRegressor)</b>	n_estimators	50, 100, 200
	Learning rate	0.01, 0.1, 0.2
	Max depth	3, 5, 7
	Subsample	0.8, 1.0

**Table 6**

Final hyperparameters obtained for each model.

Model	Hyperparameters
<b>RF</b>	100 trees (n_estimators=100), default depth and feature selection parameters
<b>XGB</b>	100 estimators (n_estimators=100), other parameters at default settings
<b>SVM</b>	C = 150, epsilon=0.05, kernel = RBF, gamma=scale
<b>ANN</b>	3 hidden layers (256-128-64), ReLU activation, Adam optimizer, learning rate = 0.001, alpha=1e-4, max_iter=8000, early stopping enabled

was also calculated and reported as error bars.

To further investigate the origin of the sample-to-sample variability in mechanical properties, a post-hoc clustering and correlation analysis was conducted using nearly the whole dataset. Here we focus on UTS as a demonstration, although the same framework can be extended to other properties. The cleaned dataset was subjected to k-means clustering based on the residuals between experimental UTS values and the smoothed temperature-dependent trend obtained by LOWESS regression. Each cluster therefore represents groups of samples exhibiting similar deviations from the minimum UTS vs. T. Finally, we performed several feature rankings, such as Spearman’s rank correlation, mutual information scores and shapley additive explanations (SHAP) based on the trained RF model, were computed between cluster membership and a combination of alloying and process parameters to identify the compositional or thermal factors most associated with high-UTS clusters.

**3. Results**

*3.1. Correlation between inputs and outputs*

Fig. 1 shows the statistical relationships between different variables and mechanical properties using Spearman correlation. We divide the plot into four correlations as below:

*3.1.1. Inter-element correlations*

The blue cluster in the top-left indicates strong positive correlation among the Cu, Al, N and their positive, but slightly weaker, correlation with other elements Ni, Ti, Si, Nb, B, Co and Cr. This suggests these elements often varied together, likely due to grade-specific formulations, e.g. higher Ni and Mo in 316, higher Ti in 321, Nb in 347. Cr shows negative correlation with Ni, Mn and Mo, reflecting compositional balancing, for instance, although Cr is high in all grades, its level is often

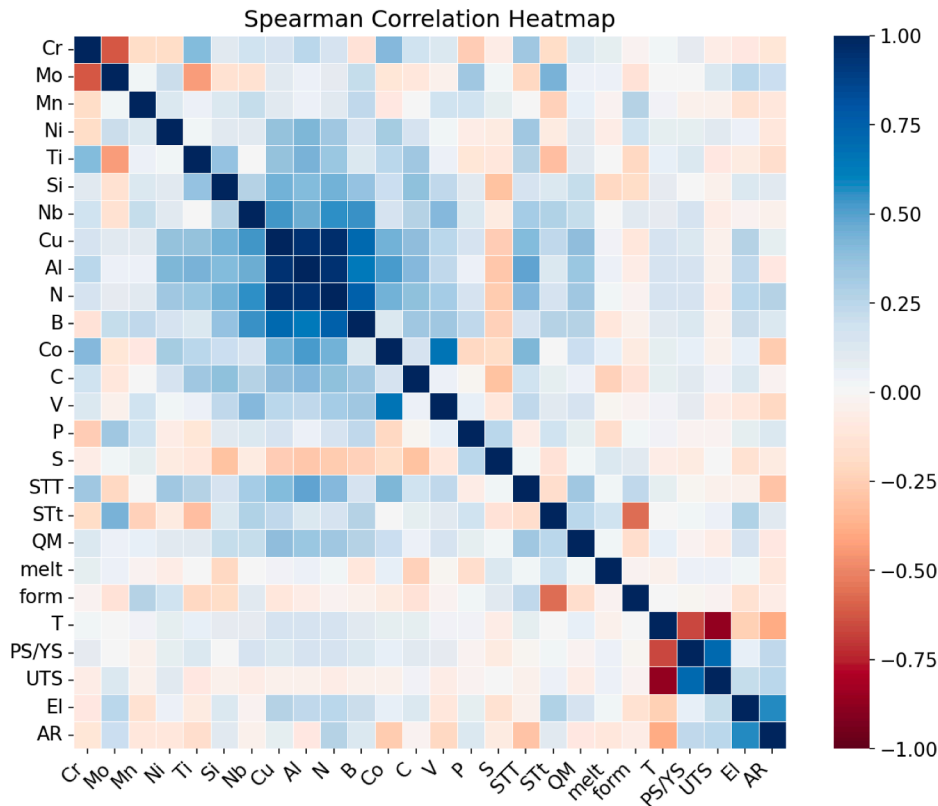


**Fig. 1.** The heatmap of correlation between composition, treatment and mechanical properties. The color scale on the right represents the range of Spearman’s rank correlation coefficient values.

reduced when Ni increases, to maintain phase stability and corrosion resistance. Additionally, Cr is relatively less expensive than Ni, Mn and Mo and is often used to reduce the overall alloy cost. It also shows negative correlation with P, B and S those are usually undesirable impurities and along with high Cr more oxidizing slags is used in refining that reduces impurities. Finally, sulfur shows a negative correlation with all element except Mo and Mn. In most stainless steels, sulfur is considered detrimental since it promotes hot shortness and reduces corrosion resistance. The more sophisticated the alloy (higher Cr, Ni, Ti, etc.), the more aggressive the refining and thus the lower the S content. Only Mn and Mo do not bind to this rule as they are added to reduce it through sulfides formation and neutralize its harmful effects. Thus, these results are consistent with established alloying principles.

### 3.1.2. Composition vs mechanical properties

Unlike temperature, none of the individual elements show a strong correlation with mechanical properties. For PS/YS and UTS, composition effect can be divided into two categories: (I) Mo, Ni, C, Mn, P and S that have similar effect on both and (II) rest of the elements that inversely affect them. In general PS/YS marks the onset of plastic deformation, while UTS represents the point at which the material can no longer withstand further stress. For this reason, they are not necessarily affected in the same way. Mechanisms such as precipitation strengthening, grain refinement and solid solution effectively increase both PS/YS and UTS by hindering dislocation motion. On the other hand, over-aged precipitates or unbalancing brittle-ductility trade-off by some solutes such as Ti and N may have opposite effect on the PS/YS and UTS.

Overall, composition shows a stronger correlation with strain targets (El and AR) than with stress targets (PS/YS and UTS). Note that AR results suffers from 70 % missing values and regardless of its strong correlation with El the imputed values are prone to errors. Nonetheless, the correlation between El and AR and composition has been a topic of debate and we refer interested readers to our earlier paper focused on the effect of composition (Kateb & Safarian, 2025).

### 3.1.3. Process & heat treatment effects

Similar to composition, variables like STT, STt, QM, melt and form show weak correlations with mechanical properties. Basic electric arc furnace is designed to refine steel by handling oxidizing slags and removing impurities, such as P and S, on an industrial scale. Induction furnace is intended for small batches of high purity alloy and normally poor refining but enables stirring for homogenous alloying. The electric furnace, in dataset probably refers to non-arc and non-induction, is mostly lab scale and does not allow effective refining and limited temperatures. Thus, one would expect stronger correlation of melt with composition, e.g. negative correlation with C, Si, B and P and being neutral to mechanical properties. General metallurgical knowledge suggests that bar shape is used for high strength application (especially cold-worked), in the middle are tube and plate those require drawing/rolling that increase overall strength by reeving grains and inducing texture while the bloom is raw shape as received from the casting of molten steel. The only notable finding is a negative correlation between form and El, suggesting that worked specimens exhibit reduced El in agreement with materials engineering principles. However, we see negligible correlation with PS/YS and UTS which can be explained by solution treatment overriding form effects. Some samples in the dataset heat treated and depending on the STT, STt, QM may have been fully recovered forming step, e.g. El positive correlation with STt and QM.

### 3.1.4. Property dependence on temperature

The correlation between temperature and mechanical properties indicates a clear sensitivity in our austenitic stainless-steel dataset. Such a strong T-correlation is far beyond what has been observed in earlier studies on the variety of steel grades (Fajrul Falaakh et al., 2024; Narayana et al., 2020; Naser, 2018; Peng et al., 2020; Shaheen et al., 2023;

Yazici & Domínguez-Gutiérrez, 2025). The fact that T is negatively correlated with all mechanical properties, does not align with thermal softening alone in which El or AR can improve on the cost of lower PS/YS and UTS. Without temperature also one would expect negative correlation of PS/YS and UTS with El (Diao et al., 2022; Kateb & Safarian, 2025). We would like to remark that our interpretations are as good as dataset. As shown in Fig. 2, within the dataset we noticed a monotonic decrease for stresses (PS/YS and UTS) but a more complex behavior for El and AR. In particular there is minima with respect to temperature, Fig. 2(c) and (d), above which strains are improved. However, in majority of data points, with the same compositions but different temperature, high temperatures are missing. This is evident from the sparse distribution of data points around 1200 K. As a result, Spearman correlation may not fully capture this relationship, since it perceives a monotonic decrease in El and AR across most of dataset.

## 3.2. Machine learning model selection and evaluation

In this study, several widely used ML models were assessed, including ANN, SVM, RF and XGB. Inspired by the human brain, ANN is well-suited for capturing complex patterns but typically demands large datasets for stable performance. SVM identifies optimal hyperplanes for classification or regression and is effective for both linear and nonlinear problems. RF constructs an ensemble of decision trees using random feature subsets, offering robustness to overfitting, minimal preprocessing and strong performance across varied data types. XGB, an advanced gradient boosting method, further enhances predictive accuracy and computational efficiency by sequentially optimizing tree-based models (Jalali et al., 2024).

Fig. 3 compares predictive performance of different models, after hyperparameter optimization, measured using the  $R^2$  score for each target mechanical properties. Error bars reflect the variations observed across the 100 random trials with 80/20 train/test split. RF and XGB demonstrate similarly strong and stable performance, for all mechanical properties. The ANN model yields lower accuracy and larger variations, particularly for El and AR, indicating reduced reliability. These findings are consistent with previous studies comparing the performance of ANN, SVM and RF on various steel grades. For PS/YS, UTS and AR, XGB shows slightly higher performance, with error bars comparable to RF. XGB's advantage likely stems from its boosting mechanism, where trees are built sequentially and corrected iteratively, an approach that tends to excel in structured datasets or those with lower noise levels. In this case, we suspect the structured nature of the data, where other grades are derived from AISI 304 by the addition of specific element(s), contributes to XGB's slight improvement in performance. However, unlike RF, XGB is highly sensitive to hyperparameter tuning and is computationally more expensive.

To ensure the robustness of the ML models and mitigate the effects of randomness, three evaluation strategies were implemented: 1-seed, 100-seeds and LOOCV. We have chosen RF for its robustness to hyperparameter tuning, i.e. mostly presenting high performance without extensive tuning. The 100-seeds approach provided insight into model consistency by averaging results across multiple random splits. In LOOCV, each data point was used once as a test sample while the remainder formed the training set, resulting in many individually trained models. Thus, LOOCV is particularly well-suited for small datasets, as it maximizes training data usage while minimizing evaluation bias. However, its computational cost increases linearly with dataset size, making it less suitable for this study. In contrast, other methods rely on random splits, which can introduce variability or bias from uneven data distribution. Here, LOOCV serves as a useful low-bias benchmark for evaluating other validation methods.

The result for RF models of mechanical properties evaluated using  $R^2$  score is shown in Fig. 4. It can be seen that almost all validation methods give scores exceeding 0.8 indicating a good performance of the model. The maximum agreement is achieved within PS/YS in which the 100-

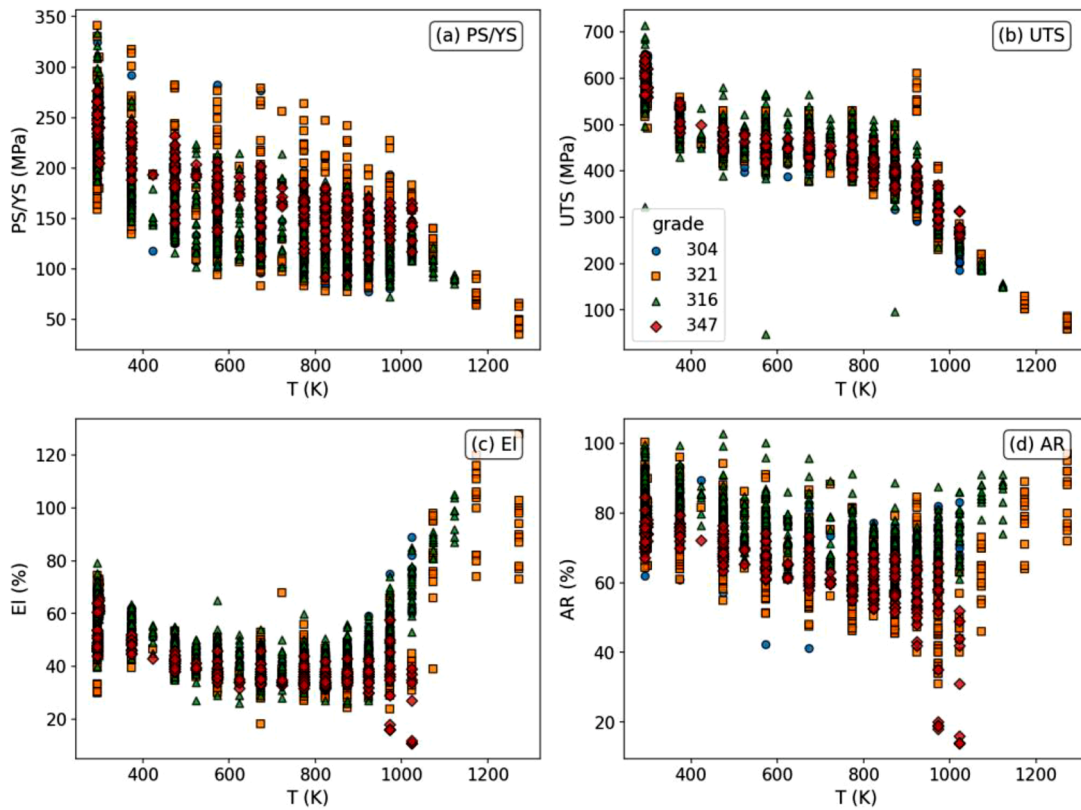


Fig. 2. Variation of mechanical properties (a) YS, (b) UTS, (c) El and (d) AR with the temperature in the dataset. The different colors indicate four austenitic stainless-steel grades 304, 316, 321 and 347.

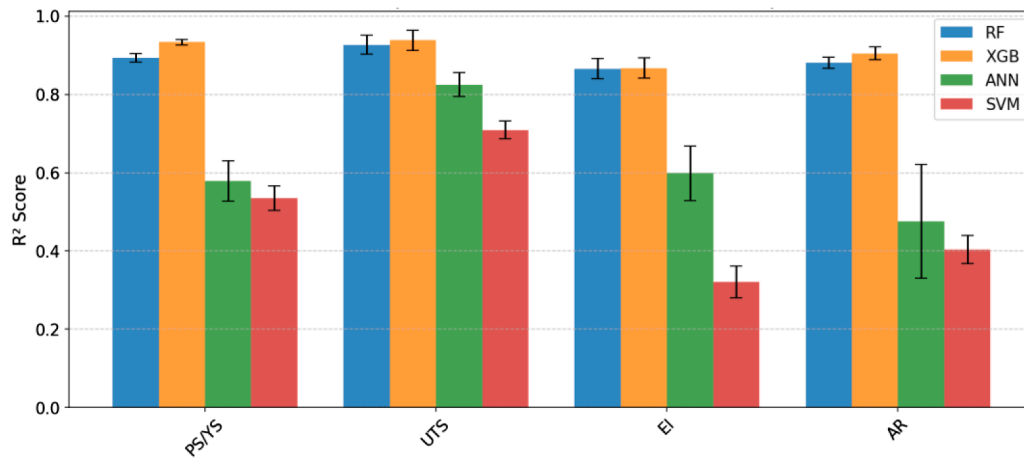


Fig. 3. Comparison of R<sup>2</sup> scores for ML models for YS, UTS, El and AR. The error bars indicate the range of scores over 100 random splits (100-seeds).

seeds error bar is relatively small and all validation methods are in close agreement. However, the 1-seed results incidentally aligns with average of 100-seeds which should not be considered a superiority as for other targets this is not the case anymore. For UTS, El and AR 1-seed indicate relatively high performance which can happen when train/test split have the same distribution of variables and targets (Kateb & Safarian, 2025). While there is always discrepancy between LOOCV and 1-seed results, the 100-seeds error bar almost overlaps with LOOCV. Thus, one may consider 100-seeds an optimal choice for validation as it stands between 1-seed and LOOCV in terms of both computational cost and accuracy.

### 3.3. Prediction of mechanical properties

Fig. 5 illustrates the scatter plots for the predicted vs experimental values for (a) PS/YS, (b) UTS, (c) El and (d) AR obtained from the 100-foldcv experiments. For each grade we used a specific color and their individual R<sup>2</sup> score indicated in the legend while total R<sup>2</sup> score is shown in label. For PS/YS and UTS, very high score has been obtained, indicating close agreement between the predicted and experimental values. The RF models effectively captured the underlying relationship between input variables and targets properties. Although for El and AR, the R<sup>2</sup> score seem relatively lower, they are much higher than the values reported in the literature (cf. Kateb and Safarian (2025) and Refs therein). Previously, we noticed a reduced accuracy by focusing on the

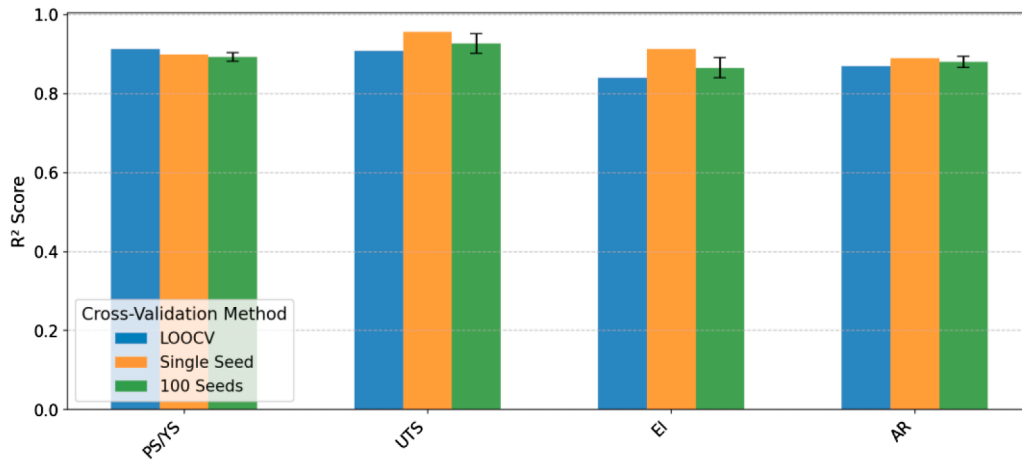


Fig. 4. Comparison of R<sup>2</sup> scores for RF models using different cross-validation strategies for the mechanical properties.

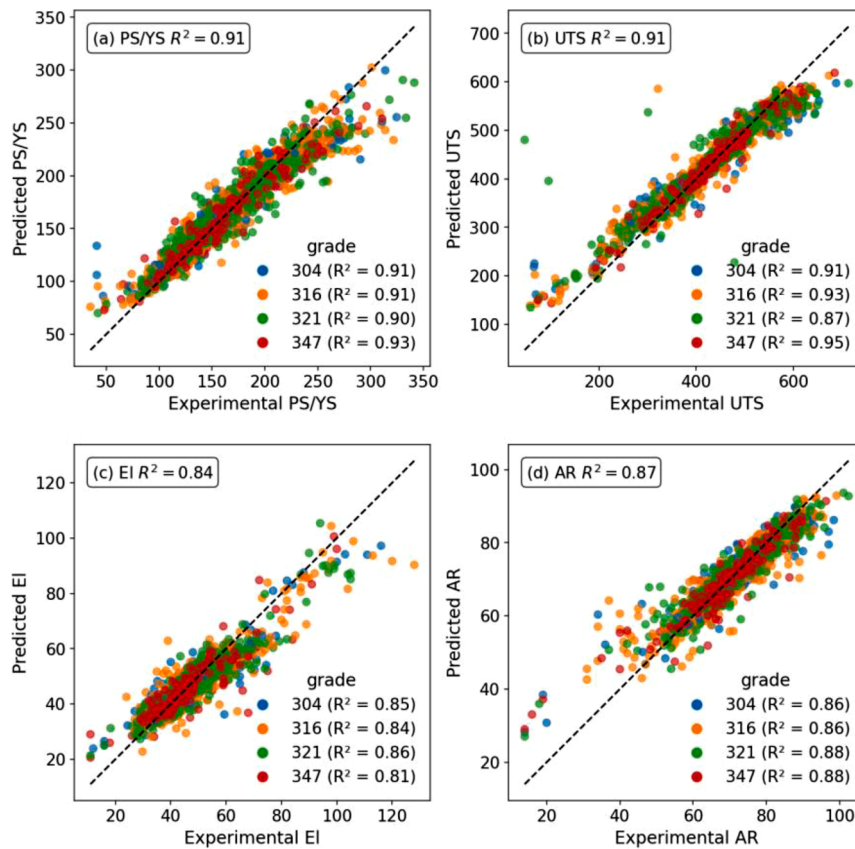


Fig. 5. Scatter plots comparing predicted and experimental values for mechanical properties using 100 fold cross-validation (a) YS, (b) UTS, (c) EI and (d) AR.

composition alone while EI present stronger correlation with process parameters. The latter has been a known issue a point of debate since development of the field. Here the dataset includes process parameters and even more but we could not reach such a good score without temperature of performing uniaxial test. This implies that the mechanical properties of austenitic stainless steels are highly sensitive to the testing temperature. We will discuss this further in the feature importance results. Remarkably, the RF model is able to capture the highly nonlinear and even non-monotonic relationship between mechanical properties and temperature (Fig. 2).

The figure also depicts different grades by different colors in Fig. 5, with their individual R<sup>2</sup> score indicated in legend while total score

indicated in the label. Since AISI 347 constitutes the majority of data points, its R<sup>2</sup> score has dominant influence on the overall model performance. For instance, lower 347 score in EI results reduces overall score and vice versa for the cases of PS/YS and UTS. Further details on the R<sup>2</sup> score obtained by different models and cross validations is presented in Table 7.

To further study how each variable affects the target properties, we performed feature importance analysis using the RF. The result for each target property is shown separately in Fig. 6. It is worth mentioning that RF does not understand positive or negative impact so it gives a measure of feature's contribution to the accuracy of the model in relation with target property. This is mainly because RF is designed for non-linear

**Table 7**  
R<sup>2</sup> score obtained by different models and cross-validation methods.

model	Validation	PS/YS	UTS	EI	AR
RF	5 fold	0.90	0.89	0.82	0.84
RF	20 fold	0.91	0.90	0.84	0.86
RF	100 fold	0.91	0.91	0.84	0.87
RF	LOOCV	0.91	0.91	0.84	0.87
RF	100-seeds	0.90	0.89	0.82	0.84
SVM	100-seeds	0.20	0.16	0.01	0.29
ANN	100-seeds	0.59	0.80	0.64	0.61
XGB	100-seeds	0.93	0.94	0.87	0.90

correlation and discovering feature interaction with the rest of features. Thus, we need to first perform RF feature importance ranking and use linear correlation to assign a positive or negative sign to it. One can argue that assigning a sign to feature that might be highly non-linear can lead to a misjudgment. As we pointed out earlier (Kateb & Safarian, 2025), this can be very good practice where due to technical reasons only some features included in the modeling and a balance of positive and negative features is necessary. Besides all features may not be necessary non-linear in the specified range which can be verified by experts in the field.

As we pointed out earlier and can be seen in all panels of the Fig. 6, the temperature of performing tensile test is the most important feature by a large margin. However, many empirical models, in same range of composition, neglected the importance of temperature (Balachandran et al., 2001; H. Nordberg, 1993; Irvine et al., 1969). Studies using ANN (Mandal et al., 2008; Shah, 2002) have shown that temperature is more than twice as influential as the second-ranked feature. An even larger gap between temperature and the next most important variable was reported by Y. C. Wang et al. (2020). In contrast, our results closely align with those of Liu et al. (2023), who used a subset of our dataset. It is also worth noting that feature importance analyses at constant temperature tend to elevate the role of alloying elements, although their relative importance remains quite small (Narayana et al., 2020).

The strong dominance of temperature in the feature importance (Fig. 6) confirms the central role of temperature in controlling mechanical properties. While Fig. 2 highlights the complex and non-linear

way in which temperature affects strength, the feature importance results provide quantitative evidence that temperature is the single most decisive factor in our dataset. This reconciles the apparent complexity of Fig. 2 with the overall trends captured by our models.

According to experts' comments we divide between different grades as indicated in the legend of Fig. 6(a). This is particularly important when working with multiple steel grades, as it helps determine whether a variable plays a key role within a specific grade or across several grades. For instance, Cr affects PS/YS and EI of all grades in the same way while it has considerably more negative effect on the UTS of AISI 321. Ti is known to improve strength by refining austenite grains and precipitation hardening even though it may have different effect on each grade (Baker, 2019; S. Wang et al., 2022; Zaitsev & Arutyunyan, 2021). We can clearly see such a behavior in PS/YS shown in Fig. 6(a). Another example is STt, solution treatment time, that changes stresses of AISI 316 more effectively than others.

An important aspect of the figure is the variability of importance for each feature, illustrated by the error bars. These represent the standard deviation of feature importance values across individual decision trees in the RF. A short error bar indicates consistent importance across trees, while error bars that span from positive to negative suggest reversal in the feature's effect that often aligns with metallurgical understanding. For example, Mo may strengthen steel through solid-solution in some compositions, but in others, it may promote carbide formation or interact with other elements in ways that reduce strength. Combining grade-specific feature importance with error bar helps prevent misinterpretation due to oversimplified assumptions. For instance, Cr, typically a ferrite stabilizer, was incorrectly described as an austenite stabilizer in one study (Y. C. Wang et al., 2020). In another case, Cr was identified as a key strengthener through carbide formation, despite the grade having too little carbon to support that mechanism (Diao et al., 2022).

The grade specific feature importance also reflects a fundamental aspect of ML interpretability, feature interactions and dataset heterogeneity. Feature importance in individual grades evaluates local behavior, where influence of features is modulated by narrower composition-processing ranges and thus may deviate from overall ones. According to Simpson's paradox, aggregated data can mislead and

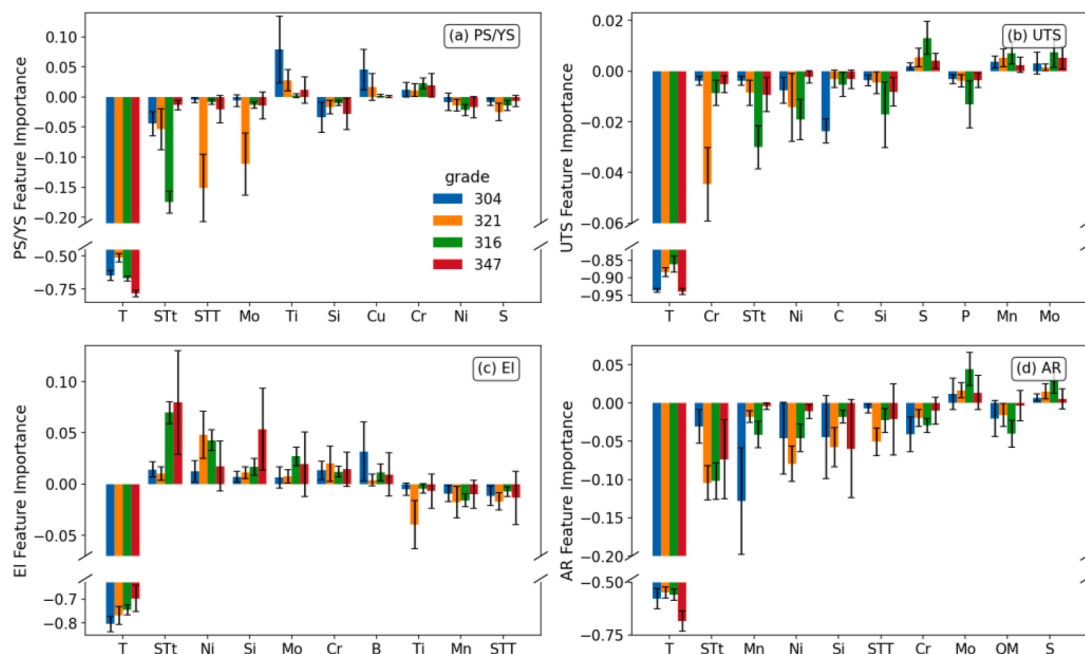


**Fig. 6.** The RF model's top 10 most influential features for each mechanical property were ranked based on their importance scores: (a) PS/YS, (b) UTS, (c) EI and (d) AR.

relationships between variables can change when considering different subgroups. In the full dataset, Nb appeared as the 4th most important feature for predicting PS/YS; however, when analyzed by individual grades, it ranked as low as 18th (not shown here).

Nonetheless, feature importance analysis suggests that most alloying and process efforts have focused on improving EI at various operation temperatures. However, there still huge demand for design of alloy/treatments that can improve stresses and AR as current features fail to enhance these properties. In particular, the feature importance of temperature for UTS is about 0.9 that means all other features have negligible influence. The later suggest need for revisiting empirical models based on the composition alone.

To explore the origin of strength variability within each steel grade, clustering was performed on the residuals of UTS relative to the minimum temperature-dependent behavior of each grade. Fig. 7(a) shows temperature dependence of UTS, where clusters are distinguished by color and steel grades by different symbols. The clustering successfully separates data points that deviate positively from the baseline at each temperature, with cluster 3 (in red) consistently exhibiting superior UTS across multiple grades and temperatures.

To understand the origin of these deviations, three complementary feature-importance analyses were performed using compositional and

process variables together with the cluster index. The results of Spearman's rank correlation, mutual information scores and SHAP analysis are presented in Fig. 7(b-d). Although the cluster index was the most influential variable in all cases, it was excluded from these plots to emphasize the effects of the remaining features. Collectively, the results indicate that no single element fully explains the high strength; rather, it likely arises from the combined influence of multiple alloying elements and optimized heat-treatment conditions.

The Spearman correlation coefficients, Fig. 7(b), show that heat-treatment time (STt) and V exhibit the strongest positive correlation with the UTS clusters, followed by Co, Mo and S. In contrast, several parameters, particularly C, display slightly negative correlations with cluster separation. The mutual information scores, Fig. 7(d), confirm the statistical relevance of these features, with Ni, Cr, STt, Mo and Mn ranking highest, reflecting their strong and non-linear relationships with the residual-based clusters. Parameters such as Si and those ranked below show intermediate or weak associations, while the mutual information score of zero for grade indicates complete independence between grade and cluster membership.

The SHAP analysis, Fig. 7(c), provides a more detailed and nonlinear interpretation of how individual features contribute to UTS prediction. A positive SHAP value corresponds to features that increase the predicted

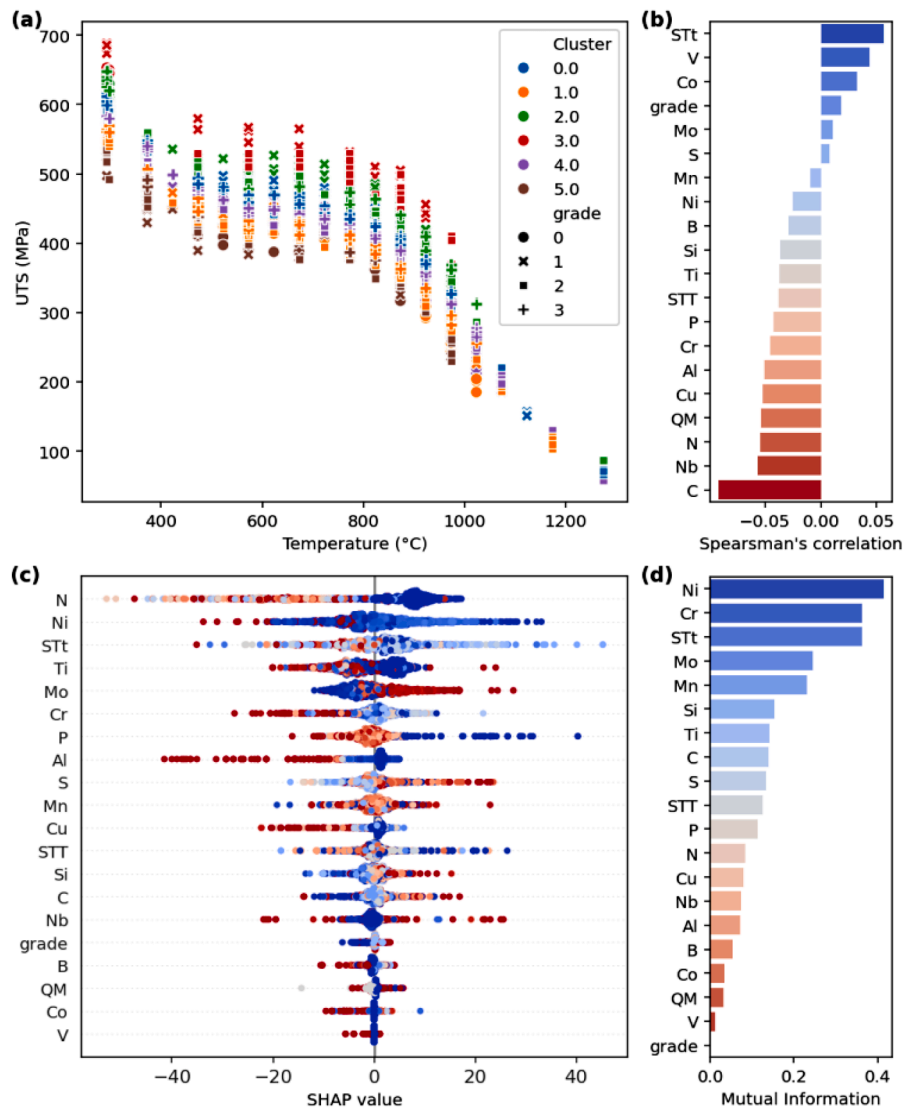


Fig. 7. (a) UTS as a function of temperature, where colors indicate clusters derived from residuals relative to the minimum of each grade. Feature-importance analyses using (b) Spearman correlation, (c) SHAP and (d) mutual information scores. For clarity, the cluster index was omitted from panels (b-d).

UTS and vice versa. Feature color indicates magnitude, with red representing higher feature values, e.g. a high Ni fraction, and blue indicating lower values. The thickness of the data bands reflects the density of samples at a given SHAP value, while the vertical order corresponds to the mean absolute SHAP magnitude. The most influential features are N, Ni, STt, Ti, Mo, and Cr. Interestingly, high values of N, Ni, STt, Ti, and Cr (as indicated by red points) associated with negative SHAP values, suggesting that excessive amounts of these variables may reduce UTS, whereas increased Mo, C, Si, and S tend to enhance strength, as indicated by red points on the positive SHAP side. Elements such as Nb appear neutral at low concentrations but show divergent effects at higher amounts. Finally, Ni and Mn exhibit broad distributions, implying that their influence on UTS may vary depending on compositional interactions and thermal history. Similarly, STT and STt do not show a single monotonic trend, highlighting the complex interplay between heat treatment and alloy chemistry discussed in the following section.

#### 4. Discussion

By defining clusters based on deviations from the minimum temperature-dependent UTS trend, we effectively isolated specimens exhibiting superior strength relative to their intrinsic baseline. Unlike conventional clustering methods applied directly to compositional variables or principal component scores, this residual-based approach emphasizes samples with higher mechanical performance at a given temperature, regardless of grade identity.

To investigate the metallurgical origins of such superior behavior, three complementary feature-importance techniques were applied to alloying and process parameters. The Spearman correlation provided a first-order monotonic measure of association, revealing generally weak linear relationships between individual elements and cluster membership, an expected outcome given the highly nonlinear and interactive nature of strengthening mechanisms in complex alloys. The mutual information score, which captures both linear and non-monotonic dependencies, identified Ni, Cr, and Mo as the most statistically relevant variables. The influence of heat-treatment duration (STt) also emerged as significant, reinforcing the importance of thermal exposure history in driving the observed scatter in UTS at similar testing temperatures.

The SHAP interpretation further extends these findings by quantifying the nonlinear and multivariate effects of each feature on UTS prediction. The SHAP analysis highlighted N, Ni, STt, Ti, Mo, and Cr as the most influential parameters. Nitrogen contributes to the high UTS primarily through three mechanisms: interstitial solid-solution strengthening, and formation of fine, dispersed precipitates such as TiN, AlN and Cr<sub>2</sub>N that effectively hinder dislocation motion and also act as grain refiners by hindering grain growth at high temperatures. Although moderate N levels are beneficial, excessive N, often introduced to partially substitute expensive Ni as an austenite stabilizer, can degrade mechanical properties. When N exceeds its solubility limit, it combines with chromium to form coarse, brittle chromium nitride at grain boundaries. However, at elevated temperatures these precipitates tend to coarsen specially at grain boundaries or form carbonitride with Nb, leading to a reduction in UTS. Such temperature-dependent precipitation and coarsening effects were not captured by the correlation-based methods, explaining the lower apparent importance of N in those analyses.

Interestingly, Ni shows a complex, non-monotonic relationship with UTS. The SHAP analysis also reveals that the percentage contributions of Ni and Mn are opposite in sign, which is understandable since Mn serves as a more economical replacement for Ni. While both are strong austenite stabilizers, Mn primarily enhances N solubility and thereby indirectly strengthens the alloy, whereas Ni's role involves a combination of phase stabilization and solution strengthening that is more context-dependent. Consequently, Mn's strengthening effect becomes more pronounced at lower temperatures, whereas Ni's contribution

varies with both composition and thermal history. The strong coupling between N and STt further indicates that N-related precipitation and diffusion processes are activated at intermediate temperatures, influencing strength evolution during heat treatment.

#### 5. Conclusions

In summary, this study shows that ML models, particularly RF, can accurately predict a complete range of mechanical properties, including nonlinear and non-monotonic temperature-dependent of targets, for various steel grades using realistic, mixed-type datasets. RF's ability to handle both numerical and categorical variables makes it especially well-suited for such complex materials data. In this investigation, RF and XGB models showed superior accuracy in predicting mechanical properties (YS, UTS, El, AR) of austenitic stainless steels, outperforming ANN and SVM, particularly under robust validation schemes. Repeated random splits and LOOCV confirmed model stability and minimal bias. Random forest-based feature analysis identified temperature as the primary determinant of tensile behavior, especially UTS, where its influence overshadowed all other inputs. Grade-specific trends and error analysis emphasized the complexity of alloy-design interactions and the limitations of conventional composition-driven models. Clustering based on the residual from minimum UTS T-dependent trend followed by feature analysis especially SHAP, further revealed the temperature-sensitive strengthening role of N. SHAP interpretation linked nitrogen's contribution to both precipitate-forming elements (Ti, Al, Cr) and heat-treatment duration, indicating its role in fine nitride or carbonitride formation that coarsens at high temperature, reducing UTS. Moreover, SHAP showed a clear coupling between N and Mn, consistent with Mn's function in increasing N solubility and partially replacing costly Ni as an austenite stabilizer. These findings challenge the adequacy of traditional composition-based empirical models for stainless steels and underscore the need to incorporate temperature and process variables into predictive frameworks. By linking data-driven insights to metallurgical mechanisms, the study demonstrates how ML interpretation can bridge predictive accuracy with physical understanding. Future work should explore targeted alloy design strategies and process optimizations to enhance ductility and strength while accounting for complex thermal effects. This study demonstrates that supervised ML can achieve high predictive performance across a complex, multi-grade stainless steel dataset. The results not only maintain robustness despite the broad parameter space but also outperform or match the accuracy reported in prior studies using either different grades or subsets of this dataset.

#### Declaration of competing interest

The authors declare that they have no known competing financial interests or personal relationships that could have appeared to influence the work reported in this paper.

#### Data availability

The data is available in link provided in the references.

#### References

- Azadeh, M., Kateb, M., & Marashi, P. (2019). Determining phase transition using potential energy distribution and surface energy of Pd nanoparticles. *Computational Materials Science*, 170, Article 109187. <https://doi.org/10.1016/J.COMMATSCI.2019.109187>
- Baker, T. N. (2019). Titanium microalloyed steels. *Ironmaking & Steelmaking*, 46(1), 1–55. <https://doi.org/10.1080/03019233.2018.1446496>
- Balachandran, G., Bhatia, M. L., Ballal, N. B., & Rao, P. K. (2001). Some theoretical aspects on designing nickel free high nitrogen austenitic stainless steels. *ISIJ International*, 41(9), 1018–1027. <https://doi.org/10.2355/ISIJINTERNATIONAL.41.1018>
- Chen, T., & Guestrin, C. (2016). Xgboost: A scalable tree boosting system. In *Proceedings of the 22nd Acm Sigkdd International Conference on Knowledge Discovery and Data Mining* (pp. 785–794).

- Colombier, L., & Hochmann, J. (1967). Stainless and heat resisting steels (Scripta Technica Ltd., Trans.). In *cir.nii.ac.jp*. Edward Arnold <https://cir.nii.ac.jp/crid/1130282268758435840>.
- Diao, Y., Yan, L., & Gao, K. (2022). A strategy assisted machine learning to process multi-objective optimization for improving mechanical properties of carbon steels. *Journal of Materials Science & Technology*, 109, 86–93. <https://doi.org/10.1016/j.jmst.2021.09.004>
- Fajrul Falaakh, D., Cho, J., & Bum Bahn, C. (2024). Machine learning approach for predicting and understanding fatigue crack growth rate of austenitic stainless steels in high-temperature water environments. *Theoretical and Applied Fracture Mechanics*, 133, Article 104499. <https://doi.org/10.1016/j.tafmec.2024.104499>
- Guo, S., Yu, J., Liu, X., Wang, C., & Jiang, Q. (2019). A predicting model for properties of steel using the industrial big data based on machine learning. *Computational Materials Science*, 160, 95–104.
- Guo, Z., & Sha, W. (2004). Modelling the correlation between processing parameters and properties of maraging steels using artificial neural network. *Computational Materials Science*, 29(1), 12–28.
- Nordberg, H. (1993). Mechanical properties of austenitic and duplex stainless steels. In *1st European Stainless Steel Conference. Processes and Materials Innovation Stainless Steel*. <https://www.tib.eu/en/search/id/TIBKAT:183323343/>.
- Irvine, J. K., Gladman, T., & Pickering, F. P. (1969). The strength of Austenitic stainless steels. *Journal of the Iron and Steel Institute*, 207, 379–390. <https://cir.nii.ac.jp/crid/1570572699423046144>.
- Jalali, S., Baniadam, M., & Maghrebi, M. (2024). Impedance value prediction of carbon nanotube/polystyrene nanocomposites using tree-based machine learning models and the Taguchi technique. *Results in Engineering*, 24, Article 103599. <https://doi.org/10.1016/j.rineng.2024.103599>
- Kateb, M., Azadeh, M., Marashi, P., & Ingvarsson, S. (2018). Size and shape-dependent melting mechanism of Pd nanoparticles. *Journal of Nanoparticle Research*, 20(9), 1–15. <https://doi.org/10.1007/S11051-018-4355-7>
- Kateb, M., & Dehghani, K. (2012). Comparison of fracture behavior of sharp with blunt crack tip in nanocrystalline materials by Molecular Dynamics simulation. *International Journal of Modern Physics: Conference Series*, 5, 410–417.
- Kateb, M., Gudmundsson, J. T., & Ingvarsson, S. (2019). Effect of atomic ordering on the magnetic anisotropy of single crystal Ni80Fe20. *AIP Advances*, 9(3), Article 35308. <https://doi.org/10.1063/1.5088602>
- Kateb, M., & Manolescu, A. (2023). *Distinct melting behaviour of partially oxidized Cu nanoparticles and nanowires*. <https://arxiv.org/pdf/2302.02219>.
- Kateb, M., Nazemi, K., & Fahime Farhani, K. D. (2009). Molecular dynamic simulation of fatigue behavior of FCC nanostructured materials. In *2nd International Conference on Ultrafine Grained and Nanostructured Materials*.
- Kateb, M., & Safarian, S. (2025). Machine learning-driven predictive modeling of mechanical properties in diverse steels. *Machine Learning with Applications*, 20, Article 100634. <https://doi.org/10.1016/J.MLWA.2025.100634>
- Liu, C., Wang, X., Cai, W., Yang, J., & Su, H. (2023). Optimal design of the Austenitic stainless-steel composition based on machine learning and genetic algorithm. *Materials*, 16, 5633. <https://doi.org/10.3390/MA16165633>
- Mandal, S., Sivaprasad, P. V., Barat, P., & Raj, B. (2009). An overview of neural network based modeling in alloy design and thermomechanical processing of austenitic stainless steels. *Materials and Manufacturing Processes*, 24(2), 219–224. <https://doi.org/10.1080/10426910802612361>
- Mandal, S., Sivaprasad, P. V., Venugopal, S., Murthy, K. P. N., & Raj, B. (2008). Artificial neural network modeling of composition–process–property correlations in austenitic stainless steels. *Materials Science and Engineering: A*, 485(1–2), 571–580. <https://doi.org/10.1016/J.MSEA.2007.08.019>
- Narayana, P. L., Lee, S. W., Park, C. H., Yeom, J. T., Hong, J. K., Maurya, A. K., & Reddy, N. S. (2020). Modeling high-temperature mechanical properties of austenitic stainless steels by neural networks. *Computational Materials Science*, 179, Article 109617. <https://doi.org/10.1016/J.COMMATSCI.2020.109617>
- Naser, M. Z. (2018). Deriving temperature-dependent material models for structural steel through artificial intelligence. *Construction and Building Materials*, 191, 56–68. <https://doi.org/10.1016/J.CONBUILDMAT.2018.09.186>
- Norström, L. (1977). The influence of nitrogen and grain size on yield strength in type AISI 316L austenitic stainless steel. *Metal Science*, 11(6), 208–212. <https://doi.org/10.1179/MSC.1977.11.6.208>
- Peng, J., Yamamoto, Y., Hawk, J. A., Lara-Curzio, E., & Shin, D. (2020). Coupling physics in machine learning to predict properties of high-temperatures alloys. *Npj Computational Materials*, 6(1), 1–7. <https://doi.org/10.1038/S41524-020-00407-2>
- Quaranta, E., & Davies, P. (2022). Emerging and innovative materials for hydropower engineering applications: Turbines, bearings, sealing, dams and waterways, and ocean power. *Engineering*, 8, 148–158.
- Rahmati, M., Kateb, M., & Marashi, P. M. (2014). Molecular dynamic simulation of Cu nanoparticle behavior during surface indentations. In *3rd International Engineering Materials & Metallurgy Conference*.
- Safarian, S. (2023). To what extent could biochar replace coal and coke in steel industries? *Fuel*, 339, Article 127401.
- Safarian, S., Ebrahimi Saryazdi, S. M., Unnthorsson, R., & Richter, C. (2020). Artificial neural network integrated with thermodynamic equilibrium modeling of downdraft biomass gasification-power production plant. *Energy*, 213, Article 118800.
- Safarian, S., Ebrahimi Saryazdi, S. M., Unnthorsson, R., & Richter, C. (2021a). Artificial neural network modeling of bioethanol production via syngas fermentation. *Biophysical Economics and Sustainability*, 6, 1–13.
- Safarian, S., Ebrahimi Saryazdi, S. M., Unnthorsson, R., & Richter, C. (2021b). Modeling of hydrogen production by applying biomass gasification: Artificial neural network modeling approach. *Fermentation*, 7(2), 71.
- Shabani, A., Aminaei, M., & Toroghinejad, M. R. (2025). Data-driven prediction of ultimate tensile strength in low alloy steel: A machine learning approach. *Computational Materials Science*, 258, Article 114045. <https://doi.org/10.1016/J.COMMATSCI.2025.114045>
- Shah, I. (2002). *Tensile properties of austenitic stainless steel*. [University of Cambridge]. <http://www.phase-trans.msm.cam.ac.uk/2002/shah/a.pdf>.
- Shah, I., & Sourmail, T. (2002). *MAP program MAP\_data\_austenitic\_stmech*. September <https://www.phase-trans.msm.cam.ac.uk/map/data/materials/austenitic.data.htm>
- Shaheen, M. A., Presswood, R., & Afshan, S. (2023). Application of machine Learning to predict the mechanical properties of high strength steel at elevated temperatures based on the chemical composition. *Structures*, 52, 17–29. <https://doi.org/10.1016/J.ISTRUC.2023.03.085>
- Shen, C., Wang, C., Wei, X., Li, Y., van der Zwaag, S., & Xu, W. (2019). Physical metallurgy-guided machine learning and artificial intelligent design of ultrahigh-strength stainless steel. *Acta Materialia*, 179, 201–214.
- Wang, C., Shen, C., Cui, Q., Zhang, C., & Xu, W. (2020a). Tensile property prediction by feature engineering guided machine learning in reduced activation ferritic/martensitic steels. *Journal of Nuclear Materials*, 529, Article 151823. <https://doi.org/10.1016/J.JNUCMAT.2019.151823>
- Wang, S., Gao, Z., Wu, G., & Mao, X. (2022). Titanium microalloying of steel: A review of its effects on processing, microstructure and mechanical properties. *International Journal of Minerals, Metallurgy and Materials*, 29(4), 645–661. <https://doi.org/10.1007/S12613-021-2399-7>
- Wang, Y., Wu, X., Li, X., Xie, Z., Liu, R., Liu, W., Zhang, Y., Xu, Y., & Liu, C. (2020b). Prediction and analysis of tensile properties of austenitic stainless steel using artificial neural network. *Metals*, 10(2), 234. <https://doi.org/10.3390/MET10020234>. 2020, Vol. 10, Page 234.
- Xie, Q., Suvarna, M., Li, J., Zhu, X., Cai, J., & Wang, X. (2021). Online prediction of mechanical properties of hot rolled steel plate using machine learning. *Materials & Design*, 197, Article 109201.
- Xiong, J., Zhang, T. Y., & Shi, S. Q. (2020). Machine learning of mechanical properties of steels. *Science China Technological Sciences*, 63(7), 1247–1255. <https://doi.org/10.1007/S11431-020-1599-5>
- Yazici, C., & Domínguez-Gutiérrez, F. J. (2025). Machine learning techniques for estimating high-temperature mechanical behavior of high strength steels. *Results in Engineering*, 25, Article 104242. <https://doi.org/10.1016/J.RINENG.2025.104242>
- Zaitsev, A., & Arutyunyan, N. (2021). Low-carbon Ti-Mo microalloyed hot rolled steels: Special features of the formation of the structural State and mechanical properties. *Metals* 2021, 11(10), 1584. <https://doi.org/10.3390/MET11101584>